Atomic qubit manipulations with an electro-optic modulator

P. J. Lee, B. B. Blinov, K. Brickman, L. Deslauriers, M. J. Madsen, R. Miller, D. L. Moehring, D. Stick, and C. Monroe

Frontiers in Optical Coherent and Ultrafast Science Center (FOCUS) and Department of Physics, University of Michigan, Ann Arbor, Michigan 48109-1120

Received December 19, 2002

We report new techniques for driving high-fidelity stimulated Raman transitions in trapped-ion qubits. An electro-optic modulator induces sidebands on an optical source, and interference between the sidebands allows coherent Rabi transitions to be efficiently driven between hyperfine ground states separated by 14.53 GHz in a single trapped $^{111}Cd^{+}$ ion. © 2003 Optical Society of America

OCIS codes: 020.7010, 020.1670, 300.6520, 270.0270.

A collection of trapped atomic ions is one of the most attractive candidates for realizing a large-scale quantum computer.[1–3] Ground-state hyperfine levels within trapped ions can be measured with essentially perfect quantum efficiency, and these qubits can be entangled by application of appropriate radiation that couples the internal levels of the ions with their collective quantum motion.[1,4–6] Such quantum logic gates are best realized with stimulated Raman transitions (SRTs), involving two phase-coherent optical fields with a frequency difference equal to the hyperfine splitting of the ion.[7–9] These fields are detuned far from the excited state, making decoherence resulting from spontaneous Raman scattering negligible, although the SRT coupling itself vanishes when the detuning becomes much larger than the excited-state fine-structure splitting.[2] We therefore desire qubit ions such as $^{111}Cd^{+}$ or $^{199}Hg^{+}$ that have a large fine-structure splitting. Such ions also exhibit a large ground-state hyperfine splitting, making it difficult to span the frequency difference with conventional acousto-optic modulators. In this Letter we describe several methods for driving SRT in trapped $^{111}Cd^{+}$ ions by use of a high-frequency electro-optic phase modulator (EOM).

The experiment is conducted in an asymmetric quadrupole rf ion trap, as described in previous work.[10] Qubits are stored in the $^{2}S_{1/2}\,|F=1, m_F=0\rangle$ and $|F=0, m_F=0\rangle$ ground-state hyperfine levels of a single trapped $^{111}Cd^{+}$ ion, with a frequency splitting of $\omega_{\mathrm{HF}} = 2\pi \times 14.53$ GHz,[11] as shown in Fig. 1(b). One measures Rabi oscillations by performing the following sequence (see Fig. 1): (i) The ion is optically pumped to the $|F=0, m_F=0\rangle$ qubit state with π-polarized radiation resonant with the $^{2}S_{1/2}(F=1) \rightarrow {}^{2}P_{3/2}(F=1)$ transition. (ii) SRTs are driven by application of the electro-optic-modulated Raman beams to the ion for time τ. (iii) The qubit state is measured by collection of the ion fluorescence from a 1-ms pulse of σ^{-}-polarized radiation resonant with the cycling transition $^{2}S_{1/2}(F=1) \rightarrow {}^{2}P_{3/2}(F=2)$. This sequence is repeated multiple times for each τ, and the Rabi frequency Ω is extracted from the averaged fluorescence oscillation in time (an example is shown in Fig. 2).

We use a frequency-quadrupled Ti:sapphire laser operating near 214.5 nm for steps (i) and (iii). For the SRT in step (ii) a 458-nm Nd:YVO_4 laser is phase modulated with a resonant EOM at $\omega_{\mathrm{HF}}/2$ and subsequently frequency summed in a buildup cavity containing a β-barium borate crystal. The blue optical field following the EOM can be written as

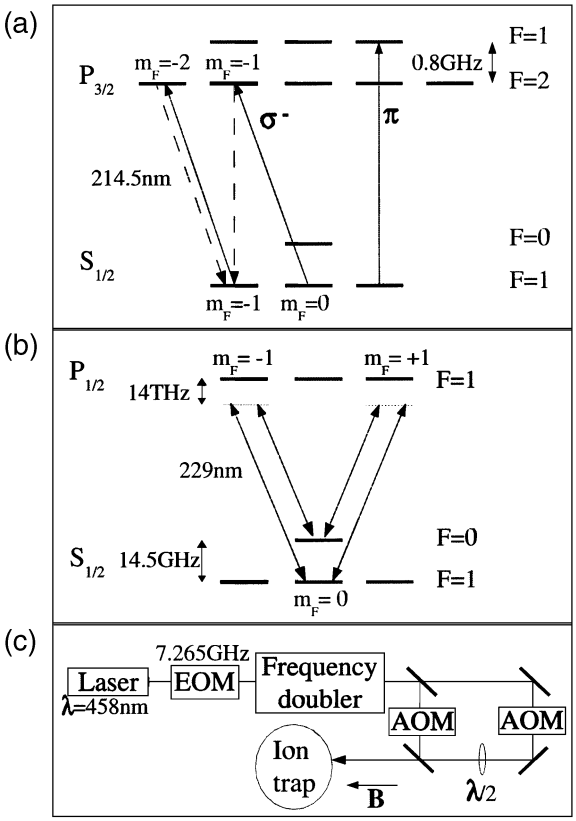

Fig. 1. (a) Relevant energy levels of a $^{111}Cd^{+}$ ion, with resonant detection (σ^{-}-polarized) and optical pumping (π-polarized) transitions indicated. (b) Coupling scheme for driving a SRT simultaneously with both $\Delta m_F = \pm 1$ couplings. (c) Schematic of the optical source for driving the SRT, including a Mach–Zehnder interferometer and acousto-optic modulator (AOM) shifters to create the frequency shift $\Delta\omega$ discussed in the text. The $\lambda/2$ plate and the external magnetic field provide constructive interference between the two paths in (b). Alternatively, the beams could be circularly polarized, with only one of the paths in (b) utilized.

0146-9592/03/171582-03$15.00/0

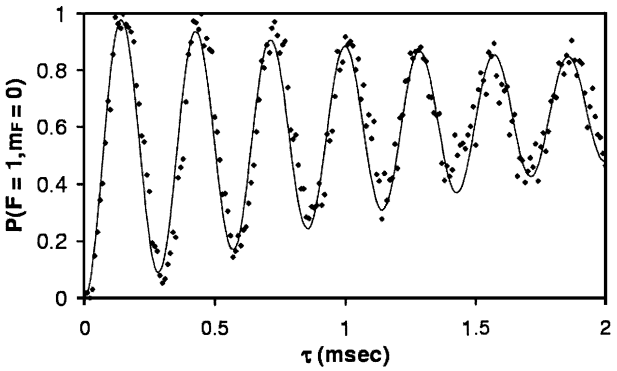

Fig. 2. Rabi flopping on a single ion by use of a SRT with 14-THz detuning. We prepare the ion in the $^2S_{1/2}$ $|F = 0, m_F = 0\rangle$ state and then pulse the Raman beams. The probability of the ion's being in the $^2S_{1/2}$ $|F = 1, m_F = 0\rangle$ state versus Raman pulse time τ is plotted, with the Rabi frequency of $\Omega \approx 2\pi \times 2$ kHz, consistent with the ~5 mW of power focused to a 20-μm waist. The decaying envelope is consistent with laser amplitude noise, and the slight upward trend is caused by residual light leakage from the resonant measuring beam, causing optical pumping. Each point represents an average of 100 experiments.

$$E_1 = \frac{E_0}{2} \exp[i(kx - \omega t)] \sum_{n=-\infty}^{\infty} J_n(\phi) \times \exp\{in[(\delta k)x - \omega_{\mathrm{HF}} t/2]\} + \text{c.c.}, \quad (1)$$

where E_0 is the unmodulated field amplitude, $J_n(\phi)$ is the nth-order Bessel function with modulation index ϕ, and $\delta k = \omega_{\mathrm{HF}}/2c$. The free spectral range (FSR) of the cavity is carefully tuned to be 1/4 of the modulation frequency so that the carrier and all the sidebands resonate simultaneously. The resulting ultraviolet radiation consists of a comb of frequencies centered at 229 nm and separated by $\omega_{\mathrm{HF}}/2$ and has an electric field

$$E_2 = \eta \frac{E_0^2}{4} \exp[2i(kx - \omega t)] \sum_{n=-\infty}^{\infty} J_n(2\phi) \times \exp\{in[(\delta k)x - \omega_{\mathrm{HF}} t/2]\} + \text{c.c.}, \quad (2)$$

where η is the harmonic conversion efficiency (assumed constant over all frequencies considered). All pairs of spectral components of the electric field separated by frequency ω_{HF} can individually drive a SRT in the ion, but the net Rabi frequency vanishes because of destructive interference. We present three schemes to modify the relative phases and amplitudes of the spectral components in Eq. (2) in order to drive the SRT.

One approach is to employ a Mach–Zehnder (MZ) interferometer, where the beam is split and recombined at another location with path-length difference Δx [see Fig. 1(c)]. The expression for the Rabi frequency is

$$\Omega = \frac{\mu_1 \mu_2 \langle E_2 E_2^* \exp(i\omega_{\mathrm{HF}} t)\rangle}{\hbar^2 \Delta} = \Omega_0 \exp[i(\delta k)(2x + \Delta x)] \sum_{n=-\infty}^{\infty} J_n(2\phi) J_{n-2}(2\phi) \times \cos\{[2k + (n-1)\delta k]\Delta x\}, \quad (3)$$

where μ_1 and μ_2 are the matrix elements of the electric dipole moment for a transition between the respective hyperfine states and the excited state, and the fields are time averaged under the rotating-wave approximation ($\Omega \ll \omega_{\mathrm{HF}} \ll \Delta$). The base Rabi frequency $\Omega_0 = \mu_1 \mu_2/(\hbar^2 \Delta)|\eta E_0^2/4|^2$ pertains to the usual case of a SRT with a pair of monochromatic Raman beams separated in frequency by ω_{HF} and each with field amplitude $\eta E_0^2/4$. For $\delta k \Delta x = (2j + 1)\pi$, where j is an integer, the Rabi frequency can be as high as $\Omega = 0.487\Omega_0$ for $\phi = 0.764$. One drawback to the form of Eq. (3) is that the $k\Delta x$ factor in the cosine requires optical stability of the MZ interferometer. This can be circumvented by introduction of a relative frequency shift $\Delta\omega \gg \Omega$ between the two paths of the MZ interferometer. One can compensate for this shift by changing the modulation frequency of the EOM by $\pm\Delta\omega/2$, resulting in a Rabi frequency of

$$\Omega = \Omega_0 \exp(-ik\Delta x)\exp[-2i(\delta k)\Delta x] \sum_{n=-\infty}^{\infty} J_n(2\phi) \times J_{n-2}(2\phi)\exp[in(\delta k)\Delta x], \quad (4)$$

where $\Delta\omega/2c \ll \delta k$. Note that the cosine term has been replaced by a phase factor $\exp(-ik\Delta x)$, thus eliminating the effects of small changes in Δx on the magnitude of the Rabi frequency. In this case the SRT Rabi frequency can be as high as $\Omega = 0.244\Omega_0$ for $\phi = 0.764$ and $\delta k \Delta x = (2j + 1)\pi$, where j is an integer.

In the experiment we set $\Delta\omega$ to be $2\pi \times 4$ MHz and measured the Rabi frequency Ω while the relative path length Δx of the MZ interferometer was varied. We fitted Ω to Eq. (4) to extract the modulation index ϕ, which was also independently measured with a Fabry–Perot spectrum analyzer. The results are plotted in Fig. 3. The dependence on gross path-length difference with spatial period $\Delta x = 2\pi/\delta k = 4.13$ cm is clearly visible.[12]

We also shaped the sideband spectrum without using a MZ interferometer by detuning the FSR of the frequency-doubling cavity slightly from a subharmonic of the EOM frequency. This detuning modifies the

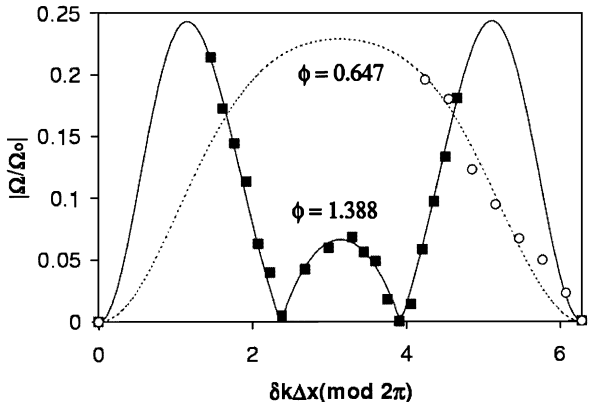

Fig. 3. Rabi frequency versus MZ path-length difference for two values of EOM modulation index ϕ. The curves are theory, and the data are fitted to Eq. (4) by use of the y-axis scale and modulation index as parameters. The fits agree with independent measurements of the modulation index with a Fabry–Perot cavity.

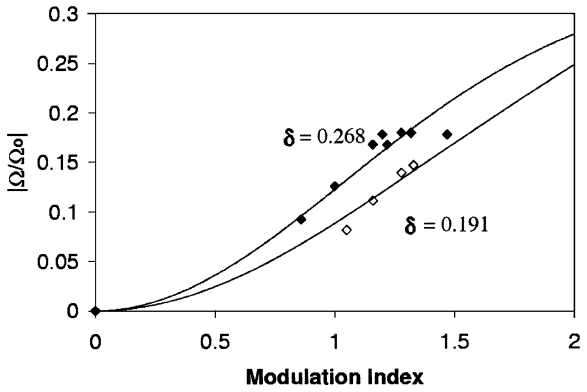

Fig. 4. Rabi frequency versus EOM modulation index for two different detunings δ of the β-barium borate buildup cavity FSR with respect to the EOM modulation frequency, scaled to the cavity linewidth (see text). The curves are theory, and the data are fitted to Eq. (5) with the y-axis scale and detuning as parameters. The fits agree with independent measurements of the cavity FSR and EOM modulation frequency.

amplitude and phase of each sideband with respect to the carrier, resulting in a Rabi frequency of

$$\Omega = 2\Omega_0 \exp[2i(\delta k)x] \sum_{n=-\infty}^{\infty} \sum_{m=-\infty}^{\infty} \sum_{l=-\infty}^{\infty} \left[\frac{J_{n-m}(\phi)}{1 - i2(n-m)\delta} \right] \times \left[\frac{J_m(\phi)}{1 - i2m\delta} \right] \left[\frac{J_{n+2-l}(\phi)}{1 + i2(n+2-l)\delta} \right] \left[\frac{J_l(\phi)}{1 + i2l\delta} \right], \tag{5}$$

where $\delta < 1$ is the number of cavity linewidths by which the first sideband is detuned from a cavity resonance. Figure 4 displays Ω versus ϕ for various cavity detunings, and the data agree with Eq. (5).

Another possible scheme involves the suppression of certain spectral components. When the FSR of the cavity is set to be $\omega_{\mathrm{HF}}/(2n+1)$, where n is an integer, only alternating sidebands will resonate. When the even or odd sidebands are selected, we find

$$\Omega_{\mathrm{even}} = \Omega_0 \exp[-2i(\delta k)x] \sum_{n=-\infty}^{\infty} \sum_{m=-\infty}^{\infty} \sum_{l=-\infty}^{\infty} J_{2(n-m)}(\phi) \times J_{2m}(\phi) J_{2(n+1-l)}(\phi) J_{2l}(\phi), \tag{6}$$

$$\Omega_{\mathrm{odd}} = \Omega_0 \exp[-2i(\delta k)x] \sum_{n=-\infty}^{\infty} \sum_{m=-\infty}^{\infty} \sum_{l=-\infty}^{\infty} J_{2(n-m)+1}(\phi) \times J_{2m+1}(\phi) J_{2(n+1-l)+1}(\phi) J_{2l+1}(\phi). \tag{7}$$

The maximum Ω_{even} is $0.230\Omega_0$ at modulation frequency $\phi = 1.173$, while the maximum Ω_{odd} is $0.279\Omega_0$ at $\phi = 1.603$.

The techniques reported here have been extended to drive a SRT between internal and motional states of trapped ions for entangling quantum logic operations. Here the modulated Raman beams are split and recombined at the ion with noncopropagating wave vectors, forming an effective MZ interferometer, as described above. In addition, the Mølmer–Sørensen bichromatic quantum logic gate scheme[5] can be implemented simply by insertion of an appropriate relative frequency shift $\Delta\omega$ between the arms of the interferometer.

In summary, we have used a high-frequency EOM to demonstrate SRT Rabi oscillations on a single trapped $^{111}Cd^+$ ion with a frequency separation of 14.53 GHz, where spontaneous emission is expected to be negligible. The techniques of shaping the sideband spectrum or creating an interference pattern between multiple modulated beams results in efficient use of the optical power for a SRT, allowing the possibility of operating high-fidelity quantum logic gates.

We acknowledge useful discussions with R. Conti, C. Rangan, and P. Haljan. This work was supported by the Advanced Research and Development Activity, National Security Agency, under U.S. Army Research Office contract DAAD19-01-1-0667 and the National Science Foundation Information Technology Research Program. P. J. Lee's e-mail address is juitl@umich.edu.

References

1. J. I. Cirac and P. Zoller, Phys. Rev. Lett. **74,** 4091 (1995).
2. D. J. Wineland, C. Monroe, W. M. Itano, D. Leibfried, B. E. King, and D. M. Meekhof, J. Res. Natl. Stand. Technol. **103,** 259 (1998).
3. D. Kielpinski, C. Monroe, and D. J. Wineland, Nature **417,** 709 (2002).
4. C. Monroe, D. M. Meekhof, B. E. King, W. M. Itano, and D. J. Wineland, Phys. Rev. Lett. **75,** 4714 (1995).
5. K. Mølmer and A. Sørensen, Phys. Rev. Lett. **82,** 1835 (1999).
6. C. A. Sackett, D. Kielpinski, B. E. King, C. Langer, V. Meyer, C. J. Myatt, M. Rowe, Q. A. Turchette, W. M. Itano, D. J. Wineland, and C. Monroe, Nature **404,** 256 (2000).
7. J. E. Thomas, P. R. Hemmer, S. Ezekiel, C. C. Leiby, Jr., R. H. Picard, and C. R. Willis, Phys. Rev. Lett. **48,** 867 (1982).
8. M. Kasevich and S. Chu, Phys. Rev. Lett. **69,** 1741 (1992).
9. C. Monroe, D. M. Meekhof, B. E. King, S. R. Jefferts, W. M. Itano, D. J. Wineland, and P. Gould, Phys. Rev. Lett. **75,** 4011 (1995).
10. B. Blinov, I. Deslauriers, P. Lee, M. Madsen, R. Miller, and C. Monroe, Phys. Rev. A **65,** 040304 (2002).
11. U. Tanaka, H. Imajo, K. Hayasaka, R. Ohmukai, M. Watanabe, and S. Urabe, Phys. Rev. A **53,** 3982 (1996).
12. M. Kasevich and S. Chu, Appl. Phys. B **54,** 321 (1992).